Batteries & Supercaps

Research Article
doi.org/10.1002/batt.202100420

Chemistry Europe
European Chemical Societies Publishing

www.batteries-supercaps.org

Ethylene Glycol as an Antifreeze Additive and Corrosion Inhibitor for Aqueous Zinc-Ion Batteries

Thuy Nguyen Thanh Tran[+],[a] Maosen Zhao[+],[b] Shujiang Geng,[b] and Douglas G. Ivey*[a]

Aqueous zinc-ion batteries are promising candidates for portable and large-scale applications because of their intrinsically high safety, low cost and high theoretical energy density. However, existing aqueous zinc-ion batteries usually suffer from zinc corrosion and poor performance at subzero temperatures. Herein, to address these problems, the electrolyte in aqueous zinc-ion batteries (1 M $ZnSO_4$) is modified by adding suitable amounts of ethylene glycol. The addition of ethylene glycol improves the antifreezing ability of the aqueous electrolyte and increases the conductivity of electrolyte at low temperatures. Ethylene glycol serves two purposes, as an antifreeze additive to significantly enhance the capacity of batteries at low temperatures and as a corrosion inhibitor to suppress zinc corrosion and byproduct precipitation. This work offers a facile strategy to realize aqueous zinc-ion batteries with good performance at low temperatures.

Introduction

In recent years, the development of grid-scale energy storage systems has stimulated demand for high-performance energy storage devices.[1] Lithium-ion batteries have demonstrated great success in commercial energy storage devices owing to their advantages of high efficiency in delivering energy, high voltage and long cycling life.[2] However, lithium-ion batteries suffer from issues such as high cost and safety problems, which hinder their large-scale application.[3] Aqueous zinc-ion batteries (AZIBs) are a promising alternative technology to lithium-ion batteries for use in large-scale applications.[4] Zinc as an ideal anode material offers several advantages, especially high capacity, nontoxicity, good safety and low cost.[5] In addition, zinc has good compatibility with aqueous electrolytes.[6]

Unfortunately, AZIBs typically exhibit unsatisfactory electrochemical performance under low-temperature conditions due to the high freezing temperature and low ionic conductivity of the aqueous $ZnSO_4$ electrolyte.[5c,7] To address this issue, several strategies, such as highly-concentrated electrolytes and hydrogel electrolytes, have been proposed to improve the electrochemical performance of low-temperature batteries.[8] Zhu et al. reported a polyacrylamide hydrogel electrolyte that retained 98% capacity upon cooling to −20 °C from room temperature.[8a] Wang et al. prepared a guar-gum/sodium-alginate/ethylene-glycol hydrogel electrolyte with excellent anti-freezing capability, which maintained a high ionic conductivity of 6.19 mS cm^{-1} at −20 °C.[9] In addition, the use of electrolyte additives, such as antifreeze additives, is a simple and straightforward method for aqueous electrolytes to overcome the poor low-temperature performance of batteries.[7b] Ethylene glycol (EG) is a well known antifreezing agent and has been widely used in automobiles and electronic devices because of its high boiling point and relatively low freezing point.[10] EG also has characteristics such as a high flash point, high dielectric constant, excellent solubility in water, low cost, low volatility and fewer safety hazards, which render it promising as an additive in aqueous electrolytes.[11] Chang et al. reported a frigostable, cost-effective, safe and eco-friendly hybrid electrolyte with high zinc ion conductivity (6.9 mS cm^{-1} at −40 °C), which was achieved by introducing EG into a 2 M $ZnSO_4$ aqueous electrolyte.[7b]

AZIBs still suffer from unsatisfactory life spans, which stem from dendritic growth and the passivation of zinc hydroxide sulfates on the anode surface, hydrogen evolution at the anode and self-corrosion of zinc metal.[12] Several strategies have been employed to address these issues. Li et al.[13] designed an 'all-in-one' (AIO) electrode by combining structural design (3D skeleton), interface modification (sufficient interface contact) and electrolyte optimization (mixed gel electrolyte). The AIO electrode can effectively suppress hydrogen evolution and side reactions, thereby achieving better stability. Li et al.[14] protected the Zn anode with a HfO_2 coating, which suppressed formation of zinc dendrites and improve electrochemical performance of zinc anodes. Xie et al.[15] successfully applied a bentonite colloidal (Ben-colloid) electrolyte in Zn/MnO_2 batteries. The Ben-colloid material covered the Zn surface during the charge/discharge process, preventing direct contact between the electrode and the electrolytes that can cause hydrogen evolution. In addition, the introduction of organic solvent additives can stabilize Zn anodes. EG as an organic additive has been shown to prevent the corrosion of zinc anodes and impede the formation of zinc hydroxide sulfates.[16]

Despite the fact that several studies have been done to investigate Mn oxides, the storage mechanisms with respect to

[a] T. Nguyen Thanh Tran,[+] Prof. D. G. Ivey
Department of Chemical and Materials Engineering
University of Alberta
Edmonton, Alberta, Canada T6G 1H9
E-mail: divey@ualberta.ca
[b] M. Zhao,[+] Prof. S. Geng
Shenyang National Laboratory for Materials Science
Northeastern University
No.3-11 Wenhua Road, Shenyang, 110819, China
[+] These authors contributed equally to this work.

Supporting information for this article is available on the WWW under https://doi.org/10.1002/batt.202100420

Research Article
doi.org/10.1002/batt.202100420
Chemistry Europe
European Chemical Societies Publishing

their electrochemical performance in AZIBs are still not well established. Specifically, H^+ insertion to form MnOOH during discharge may occur solely, simultaneously or sequentially with Zn^{2+} insertion.[17] Nevertheless, α-MnO_2 is a promising cathode for AZIBs due to its high theoretical capacity and voltage.[18] Solutions containing 2 M $ZnSO_4$ are commonly used as an electrolyte for AZIBs due to their high ionic conductivity.[19] However, α-MnO_2 suffers from severe capacity fading in 2 M $ZnSO_4$ upon cycling, due to the cathode dissolution and the formation of impurity phases.[20] α-MnO_2 demonstrates better structural stability at lower electrolyte concentrations.[20]

Herein, 1 M $ZnSO_4$ aqueous solution is used as the electrolyte for aqueous AZIBs and the solution is optimized by adding suitable amounts of EG. The freezing/melting point of the electrolyte can be controlled by adjusting the concentration of EG for different low-temperature conditions. In addition, the conductivity of the electrolyte, charge transfer impedance, rate testing of batteries at low temperatures and surface properties of the zinc electrode after cycling are investigated.

Results and Discussion

Characterization of aqueous electrolytes

Since the physical state of aqueous electrolyte solutions plays a vital role in the operation of batteries at low temperatures, the melting point (T_m) of aqueous electrolyte solutions with various concentrations of EG were investigated. As displayed in the differential scanning calorimetry (DSC) results in Figure 1, during heating, both endothermic peaks for the electrolyte with no EG (i.e., 1 M $ZnSO_4$) occur at temperatures lower than the peak for deionized water (DIW) (T_m onset at 0 °C). Onset temperature is determined as the point of intersection between the tangents with the measurement curves, whereas peak temperature is the maximum peak value on the curve at which most of the solid phase melts. The first peak for 0 EG at −10.3 °C corresponds to the eutectic melting of the binary system (water – $ZnSO_4$). The peak is immediately followed by a wider peak at −1.6 °C due to progressive melting of ice.[21] As the EG content is increased, the onset of T_m decreases to −24.5 °C, −27.9 °C, −32.5 °C and −55.8 °C for 15 EG, 20 EG, 25 EG and 30 EG, respectively. The number in front of EG corresponds to the amount of EG in % v/v. For 35 EG, there is no endothermic peak in the DSC curve, indicating that 35 EG exhibits a T_m below −65 °C, which is beneficial for low temperature battery operation. The underlying mechanism related to the effect of EG on the T_m of the electrolyte will be discussed below.

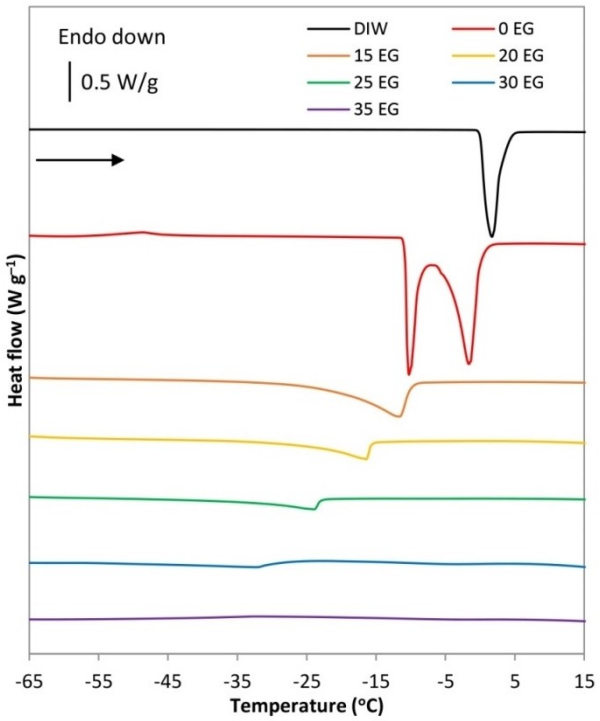

Figure 1. DSC analysis of deionized water and aqueous electrolyte solutions with antifreeze additive (EG, % v/v): 0, 15, 20, 25, 30 and 35.

It is believed that electrolyte resistance plays a crucial role in the battery and its influence becomes more significant at lower temperatures because of the increased resistance. The conductivities of aqueous electrolytes with various amounts of EG at temperatures ranging from 20 to −40 °C were investigated (Figure 2a and b). At 20 °C, increasing the EG content leads to a drop in the conductivity of the aqueous electrolytes, indicating that EG impedes Zn ion transport in the electrolyte because of the corresponding increase in viscosity.[10a] The same trend is observed when the temperature is reduced to 10 °C. However, when the temperature is below 0 °C (Figure 2b), all the EG-added electrolytes have much higher ionic conductivities than the electrolyte with no EG. In particular, the 25 EG electrolyte has the highest ionic conductivity (4.3 mS cm^{-1}) at −25 °C compared with the other electrolytes, while the conductivity of the 0 EG electrolyte drops markedly to 0.1 mS cm^{-1} (−25 °C). This is because the 0 EG electrolyte freezes at such low temperatures. Although 35 EG exhibits the lowest T_m, the viscosity of the electrolyte is increased significantly resulting in a lower conductivity than the 25 EG electrolyte. At −40 °C, the conductivity increases with increasing EG content, with the highest value (1.1 mS cm^{-1}) attained for the 35 EG electrolyte. The 35 EG electrolyte has the highest conductivity because of its reduced T_m which improves ionic mobility. The low T_m and relatively high conductivity of this electrolyte provide a possible way to fabricate high-performance AZIBs under low temperature conditions. To further confirm the stability of the electrolytes, the electrochemical stability window for the aqueous electrolytes was evaluated by linear sweep voltammetry (LSV) using graphite as the working electrode and the LSV plots are shown in Figure 2(c). The overall stability window is slightly expanded for EG-added electrolytes. It has been reported that EG expands the oxygen and hydrogen evolution potentials and enhances the thermodynamic electrochemical stability of the electrolyte to a certain extent.[10a]

Research Article
doi.org/10.1002/batt.202100420
Chemistry Europe
European Chemical Societies Publishing

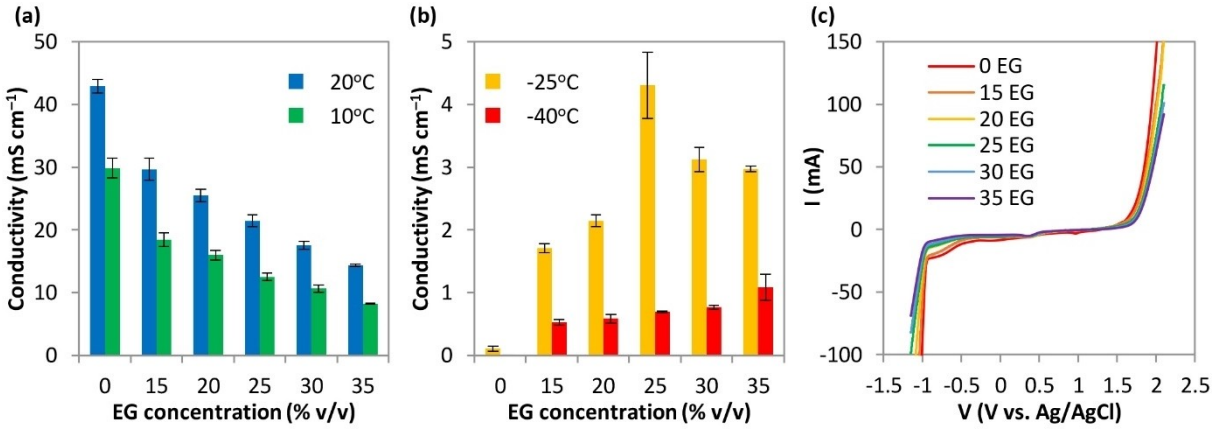

Figure 2. a, b) Conductivities of aqueous electrolytes at different temperatures and c) LSV curves for the aqueous electrolytes with stainless steel working electrodes in the potential range of -1.2 to 2 V at 20 °C.

AZIB with EG-added electrolytes

Taking into account both T_m and conductivity, 25 EG and 35 EG were selected as electrolytes to investigate cell performance. EIS measurements were conducted for the AZIB cells with the two electrolytes at different temperatures; the Nyquist plots are displayed in Figure 3. The first intercept for the Nyquist plots along the real axis represents the electrolyte resistance (R_e). The R_e values for cells with the 0 EG, 25 EG and 35 EG electrolytes are 5.5, 10.3 and 14 Ω, respectively, at 20 °C. The R_e values for the cells increase with increasing EG content at 20 °C, which is consistent with the electrolyte conductivity results. However, the R_e value for the 0 EG electrolyte increases significantly to 19 kΩ at −25 °C, which is related to the T_m of the electrolyte and its low conductivity at low temperature (Figure 2b). In sharp contrast, the cell with the 25 EG electrolyte has a much lower R_e value (95 Ω) at −25 °C. At −40 °C, the cell with the 35 EG electrolyte has the lowest R_e (798 Ω). The depressed semicircle at high and medium frequencies is related to the charge transfer resistance (R_{ct}).[22] The R_{ct} value of the cell with the 0 EG electrolyte increases from 5.5 Ω to 3.67 MΩ as the temperature decreases from 20 to −25 °C. In contrast, the R_{ct} value of the cell with the 25 EG electrolyte is 28 Ω at −25 °C, which is significantly smaller than that for the cell with the electrolyte containing no EG. At −40 °C, the cell with 35 EG retains a R_{ct} value of 261 Ω. Batteries cannot operate with large R_e and R_{ct} values if there is no EG in the electrolyte, which indicates the benefit of the EG as an antifreeze additive for battery operation at low temperatures. It should be noted that the 25 EG electrolyte is a better candidate at −25 °C due to its smaller R_{ct} value. However, the 35 EG electrolyte could be more suitable at −40 °C with its smaller R_e and R_{ct} values. As such, the suitable amount of EG depends on the operating temperature range for the battery.

The rate performance of AZIB cells, with the candidate electrolytes, was tested at 20 °C and −25 °C and the results are presented in Figure 4. As shown in Figure 4(a), the AZIB cell with the 0 EG electrolyte has the best rate capability among all the cells at 20 °C. As the amount of EG is increased, the rate capability becomes worse, which is consistent with the results discussed above. When the temperature is decreased to −25 °C, AZIB cells with EG-added electrolytes have better rate

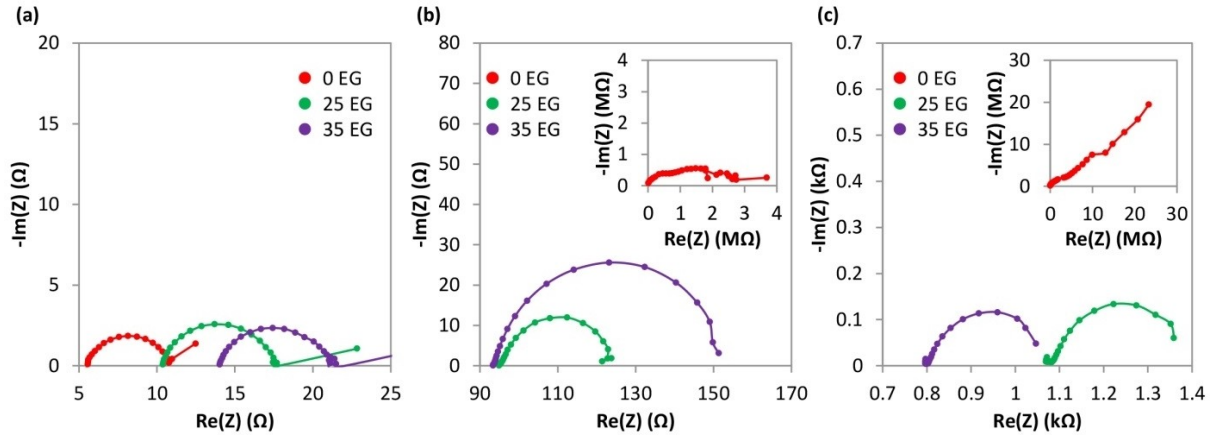

Figure 3. Nyquist plots for AZIB cells with 0 EG, 25 EG and 35 EG at temperatures of a) 20 °C, b) −25 °C and c) −40 °C.

Research Article
doi.org/10.1002/batt.202100420
Chemistry Europe
European Chemical Societies Publishing

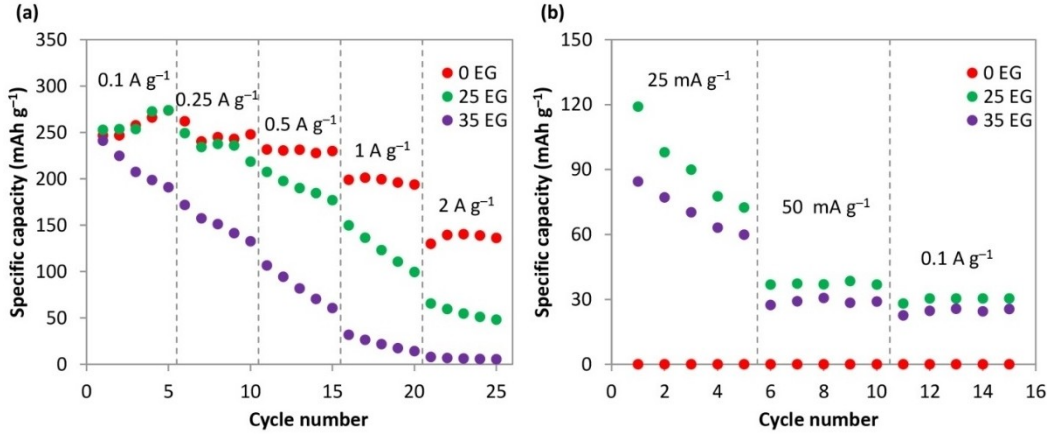

Figure 4. Rate performance of AZIB cells with 0 EG, 25 EG and 35 EG at a) 20 °C and b) −25 °C.

capabilities, while the capacity values for the battery with the 0 EG electrolyte is negligible. The cell with the 0 EG electrolyte cannot be operated at −25 °C because of the high R_e and R_{ct} values in the frozen electrolyte. It should be noted that at 0.1 A g^{-1}, the specific capacity is reduced from 250 to 30 mAh g^{-1} when the temperature drops from 20 °C to −25 °C (for the 25 EG electrolyte). Although the EIS data indicates that 35 EG has better conductivity at −40 °C, its performance at higher temperature is too low for consideration. For instance, at 0.1 A g^{-1}, the specific capacity of 35 EG gradually decreases from 240 to 190 mAh g^{-1} at 20 °C and reaches 25 mAh g^{-1} at −25 °C, which is lower than the capacity for 25 EG.

Corrosion of Zn in aqueous electrolytes

AZIB cells with 0 EG, 25 EG and 35 EG electrolytes were cycled at 0.1 A g^{-1} at 20 °C (Figure S1). The surfaces of the zinc electrodes after 20 cycles were characterized by SEM and XRD (Figures 5 and 6) to reveal the effect of EG on inhibiting zinc electrode corrosion. The Zn electrode in the cell with the 0 EG electrolyte is completely covered by particles with a sheet-like morphology. In contrast, fewer sheet-like particles are found on the surface of the Zn electrode when EG-added electrolytes are used. The EDX maps (Figure 5a) indicate that the sheet-like particles consist of Zn, O and S. The XRD patterns (Figure 6) show peaks that can be indexed to zinc (zinc electrode), as well as additional peaks which can be indexed to $Zn_4SO_4(OH)_6 \cdot xH_2O$ ($ZHS \cdot xH_2O$), where $x = 3$ or 4, which is a common byproduct at the anode side.[12b,23] The $ZHS \cdot xH_2O$ peaks decrease in intensity as more EG is added to the electrolyte, which correlates with the SEM/EDX analysis. $ZHS \cdot xH_2O$ precipitation on the zinc electrode surface can lead to problems with the AZIB.[16b] In addition to the corrosion of zinc metal, $ZHS \cdot xH_2O$ increases the charge transfer resistance (R_{ct}), leading to fading of the battery capacity.[24] The addition of EG to the electrolyte can suppress $ZHS \cdot xH_2O$ formation by limiting zinc corrosion.

The influence of additive EG on the melting point of the aqueous electrolyte and corrosion of Zn electrode are schematically depicted in Figure 7. At low temperatures, the electrolyte without EG will freeze, which is ascribed to the ordered arrangement of H_2O molecules via the strengthened hydrogen bonds (HBs) among the H_2O molecules (Figure 7a, left hand side). Such an electrolyte is unable to operate in low temperature environments. When EG is added, the abundant hydroxyl groups of EG can interact with the H_2O molecules via HBs, thereby disrupting the HBs among the H_2O molecules (Figure 7b, left hand side).[7b,25] As a result, the formation of ice crystals will be hindered leading to decreased melting temperatures.[26] In addition, it is postulated that EG could interact with Zn^{2+} and disrupt the solvation interaction between Zn^{2+} and water molecules, thereby improving Zn^{2+} ion transport in the EG-added electrolytes and improving the ionic conductivity at low temperatures.[7b]

The zinc metal electrode is not thermodynamically stable when in contact with the mildly acidic $ZnSO_4$ electrolyte.[27] Over time, Zn will be oxidized to Zn^{2+} and H^+ from the aqueous electrolyte will be reduced to H_2 gas via the hydrogen evolution reaction (HER).[28] This HER process is accelerated during AZIB operation when the potential of the zinc metal is pushed to more negative values during the charge process.[29] The consumption of protons during HER will also lead to a local increase in the electrolyte pH in the vicinity of the zinc electrode.[30] As such, $ZHS \cdot xH_2O$ will precipitate on the surface of the zinc electrode, which can be summarized as Equation (1):[31]

$$4Zn^{2+} + SO_4^{2-} + 6OH^- + xH_2O = Zn_4(OH)_6(SO_4) \cdot xH_2O \quad (1)$$

These undesired reactions are related to zinc corrosion, passivation and byproduct formation. Organic additives, such as EG, can mitigate these undesired reactions.[32] When EG is added to the electrolyte, a solvation layer is formed at the zinc metal electrode-electrolyte interface (Figure 7b), which can reduce the interaction between the water solvent and the zinc metal.[33] As a result, zinc electrode corrosion and HER processes are suppressed.[34] However, the solvation layer formed on the zinc metal anode surface also makes Zn^{2+} ion transfer across

Research Article
doi.org/10.1002/batt.202100420
Chemistry Europe
European Chemical Societies Publishing

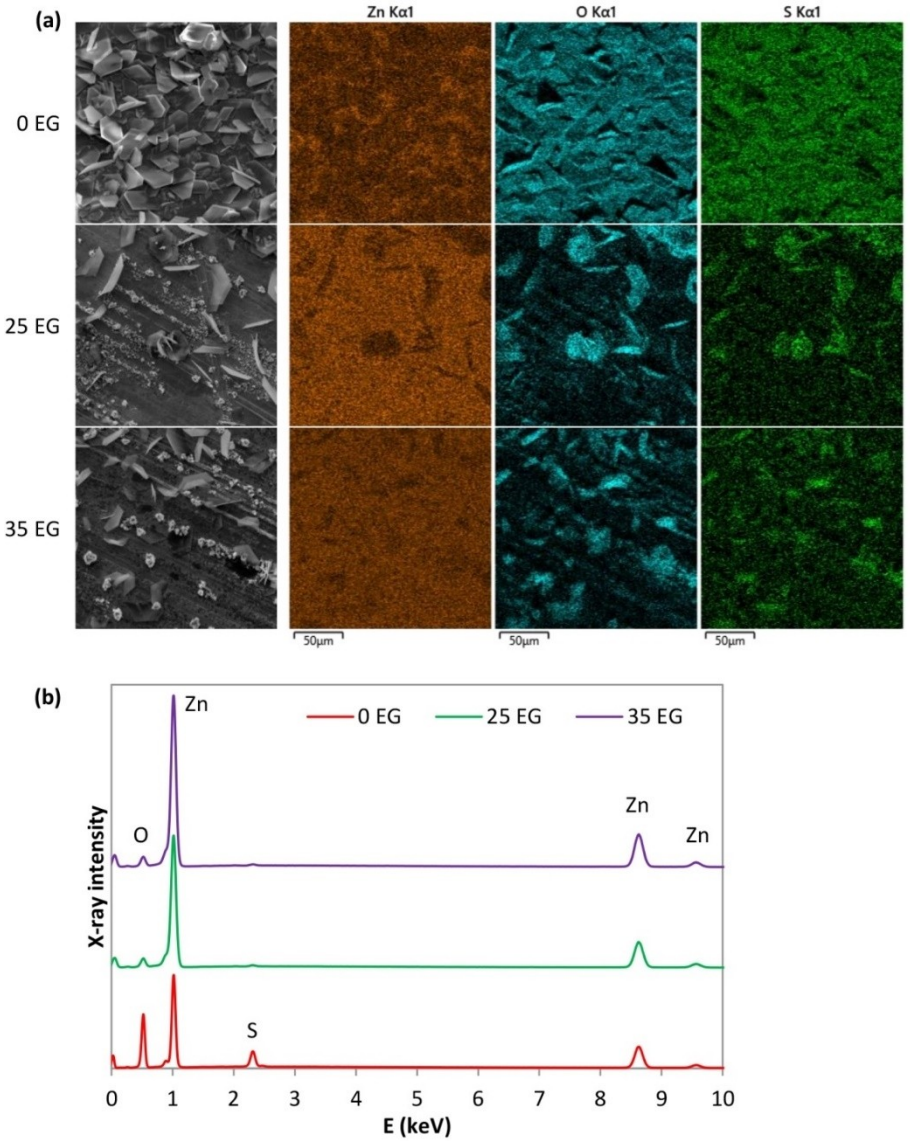

Figure 5. a) SEM secondary electron (SE) images and b) EDX spectra of Zn electrodes for the fully charged state after 20 cycles.

the interface more sluggish, leading to decreased specific cell capacity (Figure 4).[35]

On the basis of the above experimental data, ethylene glycol (EG) is identified as a promising additive for AZIBs. It can act as an antifreeze agent to improve conductivity and can be used as a corrosion inhibitor for zinc electrodes. Further studies are required to investigate the cycling behavior of AZIBs with EG additives at low temperatures.

Conclusions

A series of aqueous electrolytes (1 M $ZnSO_4$ aqueous solution) without and with the antifreeze additive ethylene glycol (EG), at various concentrations, were investigated and applied to low temperature aqueous zinc-ion batteries (AZIB). The melting point of the electrolyte can be regulated by controlling the amount of EG. The presence of EG can improve the conductivity of the electrolyte at low temperatures. The electrolyte with 25% v/v EG had a relatively high ionic conductivity of 4.3 mS cm^{-1} at −25 °C, while the electrolyte with 35% v/v EG had a conductivity of 1.1 mS cm^{-1} even at −40 °C. EG as an additive in aqueous electrolytes can improve the rate capability of batteries at subzero temperatures due to the lower bulk resistance and charge transfer resistance relative to EG-free electrolytes. EG-added electrolytes can also effectively enhance the interfacial stability between the zinc electrode and electrolyte, suppress the corrosion of zinc and suppress $ZHS \cdot xH_2O$ precipitation.

Research Article
doi.org/10.1002/batt.202100420
Chemistry Europe
European Chemical Societies Publishing

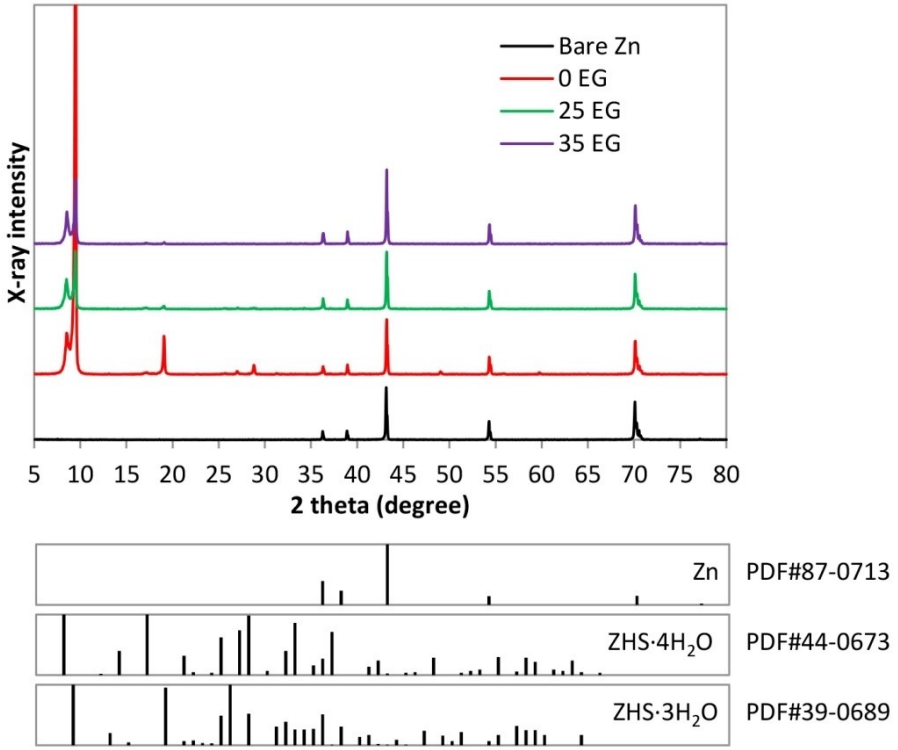

Figure 6. XRD patterns of the zinc electrodes for the fully charged state after 20 cycles.

Experimental Section

Materials preparation

All chemicals in this work were used as received, without further purification. Zinc foil (from McMaster-Carr) was used as the negative electrode. Deionized water (DIW) was used to rinse electrodes and prepare solutions. α-MnO_2, provided by Salient Energy Inc., was utilized to prepare positive electrodes for AZIBs by spraying the ink suspension onto carbon paper substrates. The ink consisted of 10 mg of α-MnO_2 powder and 5 mg of carbon black dispersed in 0.5 mL of DIW, 0.5 mL of ethanol and 50 μL of 10 wt% polytetrafluoroethylene (PTFE) (DISP30). The mass loading of α-MnO_2 on the carbon paper was approximately 2 mg cm^{-2} after drying in air overnight.

Zinc sulfate heptahydrate ($ZnSO_4 \cdot 7H_2O$) was purchased from Sigma-Aldrich for use in the electrolyte. All aqueous electrolyte solutions consisted of 1 M $ZnSO_4$ in DIW with an antifreeze additive of ethylene glycol (from Fisher) at various contents (% v/v) of 0, 15, 20, 25, 30 and 35, which are denoted as 0 EG, 15 EG, 20 EG, 25 EG, 30 EG and 35 EG, respectively.

Electrochemical measurements

Electrochemical measurements were carried out with Biologic SP-300 and VSP-300 potentiostats. Linear sweep voltammetry (LSV) of the electrolytes with different EG contents, at a scan rate of 10 mV s^{-1}, was carried out with a three-electrode system where graphite was used as working electrode, stainless steel as counter electrode and Hg/HgO as reference electrode. Conductivities of the electrolytes were measured by electrochemical impedance spectroscopy (EIS) at open circuit potential with an applied 10 mV AC potential from 100 kHz to 10 mHz. The electrolytes were contained within SS coin cells (CR2032, MTI Corporation) as shown in Figure S2a. The extracted resistance values were converted to ionic conductivity using Equation (2):

$$\sigma = \frac{L}{R \times A} \tag{2}$$

where L is the thickness of the sample (cm), A is the contact area of the small cap (cm^2) and R is the bulk resistance (mΩ). EIS was also performed at 1.2 V vs. Zn/Zn^{2+} with a 10 mV AC potential from 100 kHz to 10 mHz in full cell AZIBs. AZIB cells were assembled using a homemade plate design as shown in Figure S2b. For low temperature study, coin cells and AZIBs were refrigerated at −25 °C or −40 °C overnight.

For rate testing at room temperature, AZIBs were measured by a galvanostatic method at a series of current densities of 0.1, 0.25, 0.5, 1 and 2 A g^{-1}. At −25 °C, AZIBs were tested at 0.025, 0.05 and 0.1 A g^{-1}. For cycling tests, AZIBs were discharged to 1 V at 0.1 A g^{-1} at room temperature. During charge, AZIBs were held at 1.8 V until the current density dropped to 1 μA mg^{-1} or for an additional 2 h, whichever came first.

Materials characterization

The melting point of the aqueous electrolytes was determined using a TA Instruments Q1000 differential scanning calorimeter (DSC) under N_2 atmosphere. Specifically, an electrolyte sample (2 mg) was sealed in an aluminum sample pan which was compared with a blank pan as reference. During the measurement, both pans were first cooled to −80 °C at a cooling rate of 5 °C min^{-1}, then equilibrated at −80 °C for 10 min. Data was collected when the temperature was increased from −65 °C to 15 °C at a heating rate of 5 °C min^{-1}. After cycling tests, the surface

Research Article
doi.org/10.1002/batt.202100420
Chemistry Europe
European Chemical Societies Publishing

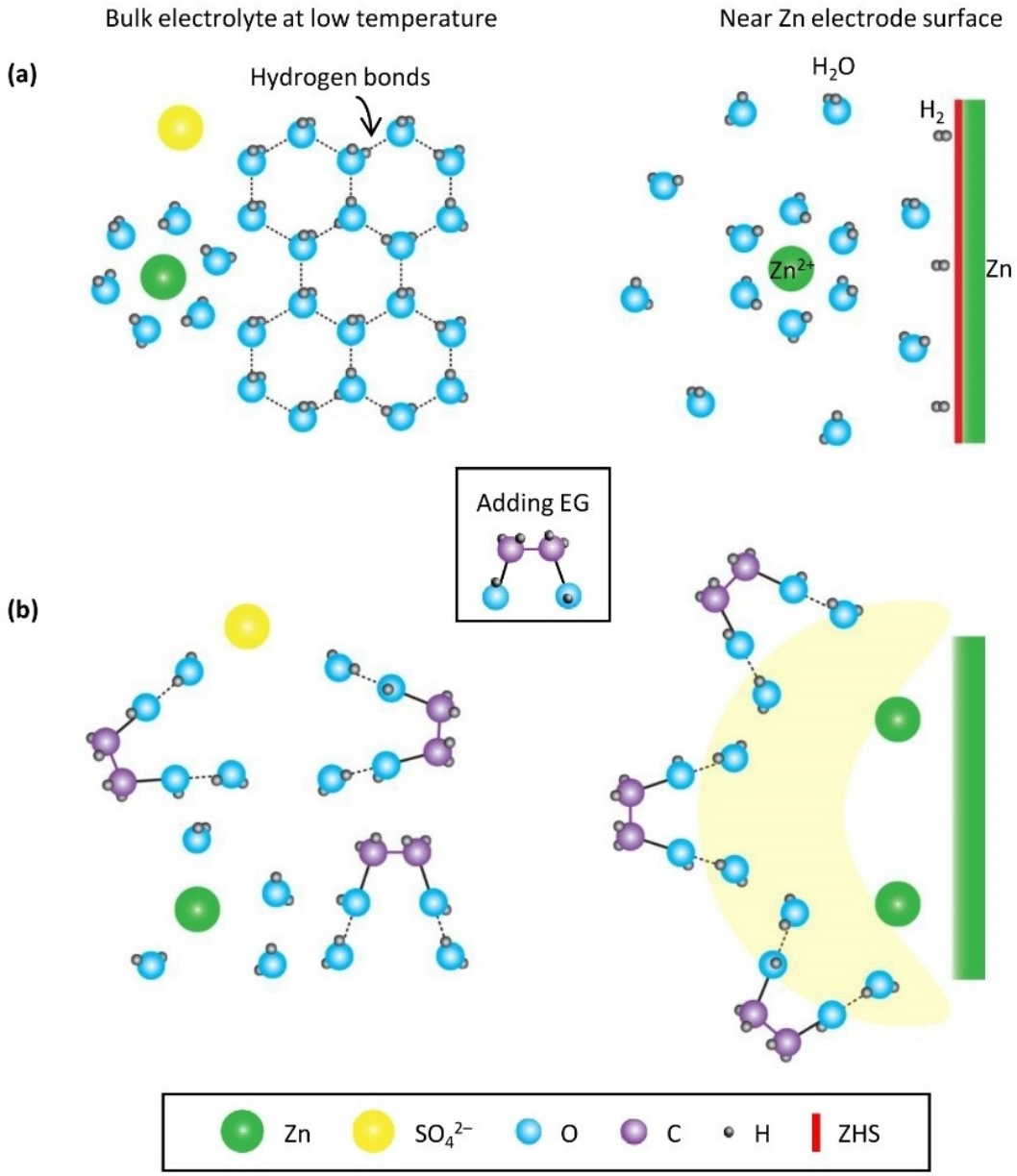

Figure 7. Schematic illustration of the mechanism showing how EG impacts the melting point of an aqueous electrolyte and the corrosion of a Zn electrode. a) Without EG and b) with the addition of EG. The yellow band represents the barrier Zn^{2+} ions must overcome to be transported through the electrolyte.

morphology and compositions of Zn electrodes were characterized using a scanning electron microscope (Tescan Vega3 SEM) coupled with an energy dispersive X-ray (EDX) spectrometer. X-ray diffraction (XRD) analysis was performed in a 2θ range of 5–80° at a scan rate of 5 degrees min^{-1} using a Rigaku Ultima IV instrument with monochromatic Cu K_α X-radiation.

Author contributions

T.N.T.T. conceived the ideas, carried out experiments, analyzed data and wrote the Experimental section. M.Z. assisted in electrochemical measurements and drafted the manuscript. S.G. and D.G.I. provided critical revisions to the manuscript. All authors have given approval to the final version of the manuscript.

Acknowledgements

The authors are grateful to the Natural Sciences and Engineering Research Council (NSERC, RGPIN-2018-04488) of Canada for providing research funding and to the Chinese Scholarship Council for supporting M. Zhao's research at the University of Alberta. Salient Energy is is also acknowledged for providing the MnO_2 powder.

Conflict of Interest

The authors declare no competing interests.

Data Availability Statement

The data that support the findings of this study are available from the corresponding author upon reasonable request.

Keywords: electrolyte · low-temperature physics · zinc · znic-ion batteries · $ZnSO_4$

[1] a) A. Konarov, N. Voronina, J. H. Jo, Z. Bakenov, Y. K. Sun, S. T. Myung, *ACS Energy Lett.* **2018**, *3*, 2620–2640; b) L. Chen, Q. An, L. Mai, *Adv. Mater. Interfaces* **2019**, *6*, 1900387.
[2] V. Etacheri, R. Marom, R. Elazari, G. Salitra, D. Aurbach, *Energy Environ. Sci.* **2011**, *4*, 3243.
[3] L. Lu, X. Han, J. Li, J. Hua, M. Ouyang, *J. Power Sources* **2013**, *226*, 272–288.
[4] a) P. Yu, Y. Zeng, H. Zhang, M. Yu, Y. Tong, X. Lu, *Small* **2019**, *15*, e1804760; b) X. Zeng, J. Hao, Z. Wang, J. Mao, Z. Guo, *Energy Storage Mater.* **2019**, *20*, 410–437.
[5] a) H. Li, L. Ma, C. Han, Z. Wang, Z. Liu, Z. Tang, C. Zhi, *Nano Energy* **2019**, *62*, 550–587; b) W. Xu, Y. Wang, *Nano-Micro Lett.* **2019**, *11*, 90; c) K. Wu, J. Huang, J. Yi, X. Liu, Y. Liu, Y. Wang, J. Zhang, Y. Xia, *Adv. Energy Mater.* **2020**, *10*, 1903977.
[6] L. E. Blanc, D. Kundu, L. F. Nazar, *Joule* **2020**, *4*, 771–799.
[7] a) A. Wang, W. Zhou, A. Huang, M. Chen, Q. Tian, J. Chen, *J. Colloid Interface Sci.* **2021**, *586*, 362–370; b) N. Chang, T. Li, R. Li, S. Wang, Y. Yin, H. Zhang, X. Li, *Energy Environ. Sci.* **2020**, *13*, 3527–3535; c) Z. Liu, X. Luo, L. Qin, G. Fang, S. Liang, *Adv. Powder Mater.* **2022**, 1, 100011.
[8] a) M. Zhu, X. Wang, H. Tang, J. Wang, Q. Hao, L. Liu, Y. Li, K. Zhang, O. G. Schmidt, *Adv. Funct. Mater.* **2019**, *30*, 1907218; b) Q. Zhang, Y. Ma, Y. Lu, L. Li, F. Wan, K. Zhang, J. Chen, *Nat. Commun.* **2020**, *11*, 4463.
[9] J. Wang, Y. Huang, B. Liu, Z. Li, J. Zhang, G. Yang, P. Hiralal, S. Jin, H. Zhou, *Energy Storage Mater.* **2021**, *41*, 599–605.
[10] a) A. Tron, S. Jeong, Y. D. Park, J. Mun, *ACS Sustainable Chem. Eng.* **2019**, *7*, 14531–14538; b) S. M. Peyghambarzadeh, S. H. Hashemabadi, S. M. Hoseini, M. Seifi Jamnani, *Int. Commun. Heat Mass Transfer* **2011**, *38*, 1283–1290.
[11] C. Ramasamy, J. Palma del Val, M. Anderson, *J. Power Sources* **2014**, *248*, 370–377.
[12] a) Y. Yu, W. Xu, X. Liu, X. Lu, *Adv. Sustainable Syst.* **2020**, *4*, 2000082; b) C. Li, X. Xie, S. Liang, J. Zhou, *Energy Environ. Mater.* **2020**, *3*, 146–159.
[13] C. Li, X. Xie, H. Liu, P. Wang, C. Deng, B. Lu, J. Zhou, S. liang, *Natl. Sci. Rev.* **2022**, *9*, nwab177.
[14] B. Li, J. Xue, C. Han, N. Liu, K. Ma, R. Zhang, X. Wu, L. Dai, L. Wang, Z. He, *J. Colloid Interface Sci.* **2021**, *599*, 467–475.
[15] X. Xie, H. Fu, Y. Fang, B. Lu, J. Zhou, S. Liang, *Adv. Energy Mater.* **2021**, *12*, 2102393.
[16] a) A. Mitha, H. Mi, W. Dong, I. S. Cho, J. Ly, S. Yoo, S. Bang, T. K. A. Hoang, P. Chen, *J. Electroanal. Chem.* **2019**, *836*, 1–6; b) V. Verma, S. Kumar, W. Manalastas, M. Srinivasan, *ACS Energy Lett.* **2021**, *6*, 1773–1785.
[17] a) Q. Zhao, X. Chen, Z. Wang, L. Yang, R. Qin, J. Yang, Y. Song, S. Ding, M. Weng, W. Huang, J. Liu, W. Zhao, G. Qian, K. Yang, Y. Cui, H. Chen, F. Pan, *Small* **2019**, *15*, 1904545; b) J. Huang, Z. Wang, M. Hou, X. Dong, Y. Liu, Y. Wang, Y. Xia, *Nat. Commun.* **2018**, *9*, 2906; c) H. Pan, Y. Shao, P. Yan, Y. Cheng, K. Han, Z. Nie, C. Wang, J. Yang, X. Li, P. Bhattacharya, K. Mueller, J. Liu, *Nat. Energy* **2016**, *1*, 16039.
[18] a) M. H. Alfaruqi, J. Gim, S. Kim, J. Song, J. Jo, S. Kim, V. Mathew, J. Kim, *J. Power Sources* **2015**, *288*, 320–327; b) Y. Huang, J. Mou, W. Liu, X. Wang, L. Dong, F. Kang, C. Xu, *Nano-Micro Lett.* **2019**, *11*, 49; c) Z. Liu, L. Qin, X. Chen, X. Xie, B. Zhu, Y. Gao, M. Zhou, G. Fang, S. Liang, *Mater. Today* **2021**, *22*, 100851.
[19] C. Xu, Y. Chen, S. Shi, J. Li, F. Kang, D. Su, *Sci. Rep.* **2015**, *5*, 14120.
[20] A. S. Poyraz, J. Laughlin, Z. Zec, *Electrochim. Acta* **2019**, *305*, 423–432.
[21] a) C. Dalmazzone, C. Noïk, D. Clausse, *Oil Gas Sci. Technol.* **2009**, *64*, 543–555; b) T. Vielma, J. Salminen, U. Lassi, *Calphad* **2018**, *60*, 126–133.
[22] A. Wang, W. Zhou, A. Huang, M. Chen, J. Chen, Q. Tian, J. Xu, *J. Colloid Interface Sci.* **2020**, *577*, 256–264.
[23] C. Deng, X. Xie, J. Han, Y. Tang, J. Gao, C. Liu, X. Shi, J. Zhou, S. Liang, *Adv. Funct. Mater.* **2020**, *30*, 2000599.
[24] T. Zhang, Y. Tang, S. Guo, X. Cao, A. Pan, G. Fang, J. Zhou, S. Liang, *Energy Environ. Sci.* **2020**, *13*, 4625–4665.
[25] R. M. Kumar, P. Baskar, K. Balamurugan, S. Das, V. Subramanian, *J. Phys. Chem. A* **2012**, *116*, 4239–4247.
[26] M. Chen, W. Zhou, A. Wang, A. Huang, J. Chen, J. Xu, C. P. Wong, *J. Mater. Chem. A* **2020**, *8*, 6828–6841.
[27] W. Manalastas Jr., S. Kumar, V. Verma, L. Zhang, D. Yuan, M. Srinivasan, *ChemSusChem* **2019**, *12*, 379–396.
[28] J. Zhao, J. Zhang, W. Yang, B. Chen, Z. Zhao, H. Qiu, S. Dong, X. Zhou, G. Cui, L. Chen, *Nano Energy* **2019**, *57*, 625–634.
[29] a) B. Beverskog, I. Puigdomenech, *Corros. Sci.* **1997**, *39*, 107–114; b) K. A. Persson, B. Waldwick, P. Lazic, G. Ceder, *Phys. Rev. B* **2012**, *85*; c) A. Jain, S. P. Ong, G. Hautier, W. Chen, W. D. Richards, S. Dacek, S. Cholia, D. Gunter, D. Skinner, G. Ceder, K. A. Persson, *APL Mater.* **2013**, *1*, 011002.
[30] J. Hao, X. Li, S. Zhang, F. Yang, X. Zeng, S. Zhang, G. Bo, C. Wang, Z. Guo, *Adv. Funct. Mater.* **2020**, *30*, 2001263.
[31] T. N. T. Tran, S. Jin, M. Cuisinier, B. D. Adams, D. G. Ivey, *Sci. Rep.* **2021**, *11*, 20777.
[32] a) Z. Hou, X. Zhang, X. Li, Y. Zhu, J. Liang, Y. Qian, *J. Mater. Chem. A* **2017**, *5*, 730–738; b) J. Hao, L. Yuan, C. Ye, D. Chao, K. Davey, Z. Guo, S. Qiao, *Angew. Chem. Int. Ed.* **2021**, *60*, 7366–7375.
[33] Y. Jin, K. S. Han, Y. Shao, M. L. Sushko, J. Xiao, H. Pan, J. Liu, *Adv. Funct. Mater.* **2020**, *30*, 2003932.
[34] a) A. Mitha, A. Z. Yazdi, M. Ahmed, P. Chen, *ChemElectroChem* **2018**, *5*, 2409–2418; b) K. E. Sun, T. K. Hoang, T. N. Doan, Y. Yu, X. Zhu, Y. Tian, P. Chen, *ACS Appl. Mater. Interfaces* **2017**, *9*, 9681–9687.
[35] S. J. Banik, R. Akolkar, *J. Electrochem. Soc.* **2013**, *160*, D519–D523.

Manuscript received: December 30, 2021
Revised manuscript received: March 22, 2022
Accepted manuscript online: March 23, 2022
Version of record online: April 5, 2022